Joint Multi-User Communication and MIMO Radar Through Full-Duplex Hybrid Beamforming

Sahan Damith Liyanaarachchi, Carlos Baquero Barneto, Taneli Riihonen, Mikko Heino, and Mikko Valkama
Electrical Engineering, Faculty of Information Technology and Communication Sciences, Tampere University, Finland
email: sahan.liyanaarachchi@tuni.fi

***Abstract*—Performing joint communication and sensing in multiple-input multiple-output (MIMO) systems is important for efficiently utilizing the crowded spectrum, through providing high capacity links to the communication users, while simultaneously facilitating improved sensing capabilities. Towards this, we optimize the transmit beamforming to provide concurrent multiple beams for communication and sensing, while effectively mitigating the cross-interference between different communication users. Moreover, the receive beamforming is optimized to observe reflections from the radar targets, while also canceling the self-interference due to the required full-duplex operation. We demonstrate that MIMO processing can separate the communication users and radar targets in the angular domain. Additionally, the super-resolution provided by angle estimation allows differentiating between radar targets having the same range, but with minuscule angular separation.**

I. Introduction

Communication and sensing systems are converging towards operating at the same frequency bands, inferring radio frequency (RF) spectrum congestion and mutual interference. To overcome this challenge, a new trend referred to as the RF convergence proposes to design joint communication and sensing (JCAS) systems that efficiently manage the spectral resources [1]. The (re)use of same hardware components for both purposes has accelerated the design of these even further.

At the same time, multiple-input multiple-output (MIMO) is an increasingly important technology for both communication and sensing functionalities at mm-waves (30–300 GHz), enabling new interesting applications [2]–[4]. For communications, it can provide high capacity links to the users through spatial multiplexing. Further, MIMO processing can be used at the sensing receiver (RX) to facilitate, e.g., super-resolution direction of arrival (DoA) estimation [5].

In this work, we propose a multi-user (MU) MIMO system for JCAS operation, where the MIMO transmitter (TX) provides multiple beams for communications, while a separate additional beam concurrently senses the environment. This idea is explored in [6] for a phased array system, whereas in this article, we extend this to a true MIMO system context. This functionality is facilitated by optimizing the effective TX beam pattern, which is the combination of the baseband (BB) and RF beamforming weights, similar to [3], [7]. Additionally, the inter-user interference between different communication users is also minimized.

This research was partially supported by the Academy of Finland (grants #310991, #315858, #319994 and #328214), Nokia Bell Labs, and the Doctoral School of Tampere University. This research was also supported by the Finnish Funding Agency for Innovation through the "RF Convergence" project.

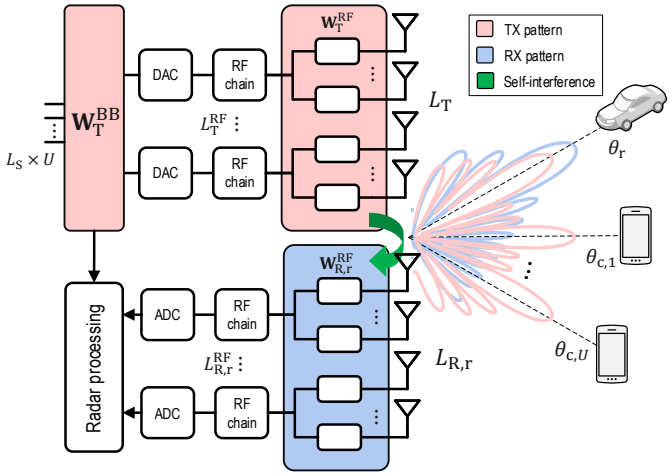

Fig. 1. Considered JCAS multi-user MIMO system.

Moreover, we have illustrated in [8] that the key enabler for future JCAS systems is the simultaneous transmit-and-receive operation, and the major challenge for implementing it is the self-interference (SI) due to the TX signal leakage to the RX. As such, the RX RF beamforming weights are optimized to minimize the SI, while providing a single beam in the sensing direction to receive the reflections from the radar targets.

We also illustrate that multiple signal classification (MUSIC) algorithm [9] can be used for DoA estimation, by utilizing properly the RX spatial signal. Specifically, we demonstrate that it can be applied for a hybrid MIMO system [10], and show how to differentiate between the different targets in the angular domain, allowing to separate multiple targets with the same range within the sensing beam. Throughout the work, we utilize orthogonal frequency-division multiplexing (OFDM) as the JCAS waveform.

II. System Model

As depicted in Fig. 1, we assume a hybrid MU-MIMO-OFDM system with U communication users. The considered JCAS system simultaneously operates as a communication TX and radar transceiver, providing communication and radar beams at $\theta_{\mathrm{c},u}$ and θ_{r}, respectively, with $u \in [1, U]$. We consider a JCAS TX with L_{T} TX antennas and $L_{\mathrm{T}}^{\mathrm{RF}}$ RF chains, while the

corresponding numbers of the RX antennas and RF chains are given by $L_{\mathrm{R,r}}$ and $L_{\mathrm{R,r}}^{\mathrm{RF}}$, respectively. We also assume uniform linear arrays (ULAs) as TX and RX antenna systems, with half-wavelength separation. The OFDM waveform contains M OFDM symbols, each having N active subcarriers. The frequency-domain symbols for the u^{th} communication user's L_{S} parallel streams at the n^{th} subcarrier and the m^{th} OFDM symbol are given by $\mathbf{x}_{u,n,m}$, of size $L_{\mathrm{S}} \times 1$.

Applying both RF and BB precoding, the TX frequency-domain symbols at the antenna elements for all the users are

$$\tilde{\mathbf{x}}_{n,m} = \mathbf{W}_{\mathrm{T}}^{\mathrm{RF}} \sum_{u=1}^{U} \mathbf{W}_{\mathrm{T},u}^{\mathrm{BB}} \mathbf{x}_{u,n,m}, \tag{1}$$

where $\tilde{\mathbf{x}}_{n,m}$ is of size $L_{\mathrm{T}} \times 1$. The TX RF precoder $\mathbf{W}_{\mathrm{T}}^{\mathrm{RF}}$ of size $L_{\mathrm{T}} \times L_{\mathrm{T}}^{\mathrm{RF}}$ is common for all users. The BB precoder of the u^{th} user is $\mathbf{W}_{\mathrm{T},u}^{\mathrm{BB}}$, which is of size $L_{\mathrm{T}}^{\mathrm{RF}} \times L_{\mathrm{S}}$. Denoting

$$\mathbf{W}_{\mathrm{T}}^{\mathrm{BB}} = \left[\mathbf{W}_{\mathrm{T},1}^{\mathrm{BB}}, \mathbf{W}_{\mathrm{T},2}^{\mathrm{BB}}, \ldots, \mathbf{W}_{\mathrm{T},U}^{\mathrm{BB}}\right], \tag{2}$$

$$\mathbf{x}_{n,m} = \left[\mathbf{x}_{1,n,m}^{T}, \mathbf{x}_{2,n,m}^{T}, \ldots, \mathbf{x}_{U,n,m}^{T}\right]^{T}, \tag{3}$$

where the BB precoder matrix of all the users $\mathbf{W}_{\mathrm{T}}^{\mathrm{BB}}$ is of size $L_{\mathrm{T}}^{\mathrm{RF}} \times (L_{\mathrm{S}} \cdot U)$ and $\mathbf{x}_{n,m}$ is the vector containing all the users' streams, of size $(L_{\mathrm{S}} \cdot U) \times 1$, (1) can be rewritten as

$$\tilde{\mathbf{x}}_{n,m} = \mathbf{W}_{\mathrm{T}}^{\mathrm{RF}} \mathbf{W}_{\mathrm{T}}^{\mathrm{BB}} \mathbf{x}_{n,m}. \tag{4}$$

A. MIMO Radar RX Signals

The RX frequency-domain symbols at the radar RX's elements due to K_{t} point target reflections can be written as

$$\begin{aligned}\tilde{\mathbf{y}}_{\mathrm{r},n,m} = &\sum_{k=1}^{K_{\mathrm{t}}} b_{\mathrm{t},k} e^{-j2\pi f_n \tau_{\mathrm{t},k}} \mathbf{a}_{\mathrm{R}}(\theta_{\mathrm{t},k}) \mathbf{a}_{\mathrm{T}}^{H}(\theta_{\mathrm{t},k}) \tilde{\mathbf{x}}_{n,m} \\ &+ \mathbf{H}_{\mathrm{SI},n} \tilde{\mathbf{x}}_{n,m} + \tilde{\mathbf{v}}_{\mathrm{r},n,m},\end{aligned} \tag{5}$$

where $b_{\mathrm{t},k}$ and $\tau_{\mathrm{t},k}$ model the attenuation factor and relative delay of the k^{th} target reflection, while $\tilde{\mathbf{v}}_{\mathrm{r},n,m}$ is the noise vector of size $L_{\mathrm{R,r}} \times 1$. The BB frequency of the n^{th} subcarrier is given by f_n. The TX and RX steering vectors are represented by $\mathbf{a}_{\mathrm{T}}(\theta_{\mathrm{t},k})$ and $\mathbf{a}_{\mathrm{R}}(\theta_{\mathrm{t},k})$, which are of sizes $L_{\mathrm{T}} \times 1$ and $L_{\mathrm{R,r}} \times 1$, respectively, while $\theta_{\mathrm{t},k}$ denotes either the angle of departure or arrival due to the k^{th} target that are equal in the considered monostatic setup – assuming for simplicity relatively far away targets and small TX-RX array separation. For an ideal ULA with L antennas and half-wavelength separation, the steering vector is given by [10]

$$\mathbf{a}(\theta) = \left[1, e^{j\pi \sin(\theta)}, \ldots, e^{j\pi(L-1)\sin(\theta)}\right]^{T}. \tag{6}$$

Representing (5) in matrix notation yields

$$\tilde{\mathbf{y}}_{\mathrm{r},n,m} = \mathbf{A}_{\mathrm{R}}(\boldsymbol{\theta}) \mathbf{H}_{\mathrm{r},n} \mathbf{A}_{\mathrm{T}}^{H}(\boldsymbol{\theta}) \tilde{\mathbf{x}}_{n,m} + \mathbf{H}_{\mathrm{SI},n} \tilde{\mathbf{x}}_{n,m} + \tilde{\mathbf{v}}_{\mathrm{r},n,m}, \tag{7}$$

where $\mathbf{A}_{\mathrm{T}}(\boldsymbol{\theta}) = [\mathbf{a}_{\mathrm{T}}(\theta_{\mathrm{t},1}), \ldots, \mathbf{a}_{\mathrm{T}}(\theta_{\mathrm{t},K_{\mathrm{t}}})]$ and $\mathbf{A}_{\mathrm{R}}(\boldsymbol{\theta}) = [\mathbf{a}_{\mathrm{R}}(\theta_{\mathrm{t},1}), \ldots, \mathbf{a}_{\mathrm{R}}(\theta_{\mathrm{t},K_{\mathrm{t}}})]$ are the TX and RX steering matrices for all the targets, of sizes $L_{\mathrm{T}} \times K_{\mathrm{t}}$ and $L_{\mathrm{R,r}} \times K_{\mathrm{t}}$, respectively. The DoAs of all the targets are denoted by $\boldsymbol{\theta} = [\theta_{\mathrm{t},1}, \ldots, \theta_{\mathrm{t},K_{\mathrm{t}}}]^{T}$. The radar channel matrix $\mathbf{H}_{\mathrm{r},n}$ is diagonal with size $K_{\mathrm{t}} \times K_{\mathrm{t}}$, and its k^{th} diagonal element is given by $(\mathbf{H}_{\mathrm{r},n})_{k,k} = b_{\mathrm{t},k} e^{-j2\pi f_n \tau_{\mathrm{t},k}}$.

In the above modeling, the SI matrix of size $L_{\mathrm{R,r}} \times L_{\mathrm{T}}$ is given by $\mathbf{H}_{\mathrm{SI},n}$, and it represents the channel between the TX and RX antenna elements, i.e., direct coupling due to full-duplex operation. After RF combining at the radar RX, the BB RX frequency-domain symbol vector of size $L_{\mathrm{R,r}}^{\mathrm{RF}} \times 1$ reads

$$\mathbf{y}_{\mathrm{r},n,m} = (\mathbf{W}_{\mathrm{R,r}}^{\mathrm{RF}})^{H} \tilde{\mathbf{y}}_{\mathrm{r},n,m}, \tag{8}$$

where $\mathbf{W}_{\mathrm{R,r}}^{\mathrm{RF}}$ is the RF combiner of size $L_{\mathrm{R,r}} \times L_{\mathrm{R,r}}^{\mathrm{RF}}$.

B. Estimation of Sensing Parameters

The RX frequency-domain symbols are given combining (4), (7) and (8) as

$$\mathbf{y}_{\mathrm{r},n,m} \simeq \underbrace{(\mathbf{W}_{\mathrm{R,r}}^{\mathrm{RF}})^{H} \mathbf{A}_{\mathrm{R}}(\boldsymbol{\theta}) \mathbf{H}_{\mathrm{r},n} \mathbf{A}_{\mathrm{T}}^{H}(\boldsymbol{\theta}) \mathbf{W}_{\mathrm{T}}^{\mathrm{RF}} \mathbf{W}_{\mathrm{T}}^{\mathrm{BB}}}_{\mathbf{A}_n(\boldsymbol{\theta})} \mathbf{x}_{n,m} + \mathbf{v}_{\mathrm{r},n,m}, \tag{9}$$

where $\mathbf{v}_{\mathrm{r},n,m}$ represents the noise vector. In this subsection, the effect of SI on the RX symbols is assumed to be negligible due to the SI cancellation method described in Section III-B, and thus neglected in the radar processing. Additionally, the matrix $\mathbf{A}_n(\boldsymbol{\theta})$ of size $L_{\mathrm{R,r}}^{\mathrm{RF}} \times (L_{\mathrm{S}} \cdot U)$ denotes the effective radar channel between the TX streams and the RX symbols.

Based on these RX symbols, the K_{t} targets' delays and DoAs that need to be estimated are given by

$$\boldsymbol{\alpha} = [\underbrace{\tau_{\mathrm{t},1}, \ldots, \tau_{\mathrm{t},K_{\mathrm{t}}}}_{\boldsymbol{\tau}}, \underbrace{\theta_{\mathrm{t},1}, \ldots, \theta_{\mathrm{t},K_{\mathrm{t}}}}_{\boldsymbol{\theta}}]^{T}. \tag{10}$$

The RX symbols in (9) are separately used for range-profile estimation [11], and DoA estimation using MUSIC [9].

1) Range-Profile Estimation: For the l^{th} RX RF chain and $l_{\mathrm{S}}^{\mathrm{th}}$ TX stream, with $l \in [1, L_{\mathrm{R,r}}^{\mathrm{RF}}]$ and $l_{\mathrm{S}} \in [1, L_{\mathrm{S}} \cdot U]$, the relation between the TX and RX frequency-domain symbols can be written based on (9) as

$$y_{\mathrm{r},n,m,l} = \sum_{l_{\mathrm{S}}=1}^{L_{\mathrm{S}} \cdot U} a_{n,l,l_{\mathrm{S}}} x_{n,m,l_{\mathrm{S}}} + v_{\mathrm{r},n,m,l}, \tag{11}$$

where $x_{n,m,l_{\mathrm{S}}}$, $y_{\mathrm{r},n,m,l}$, $a_{n,l,l_{\mathrm{S}}}$, and $v_{\mathrm{r},n,m,l}$ denote a TX stream's frequency-domain symbol, a RX frequency-domain symbol, a complex coefficient to denote the effective channel, and the noise sample, respectively, with $(\mathbf{x}_{n,m})_{l_{\mathrm{S}}} = x_{n,m,l_{\mathrm{S}}}$, $(\mathbf{y}_{\mathrm{r},n,m})_{l} = y_{\mathrm{r},n,m,l}$, $(\mathbf{A}_n(\boldsymbol{\theta}))_{l,l_{\mathrm{S}}} = a_{n,l,l_{\mathrm{S}}}$, and $(\mathbf{v}_{\mathrm{r},n,m})_{l} = v_{\mathrm{r},n,m,l}$. Next, element-wise multiplication is performed to calculate $z_{n,m,l,l_{\mathrm{S}}}$ as

$$z_{n,m,l,l_{\mathrm{S}}} = y_{\mathrm{r},n,m,l} x_{n,m,l_{\mathrm{S}}}^{*}, \tag{12}$$

where $(\cdot)^{*}$ denotes complex conjugation.

The range profile is then given as

$$d_{l,l_{\mathrm{S}}}(n') = \frac{1}{M} \left| \sum_{m=0}^{M-1} \left(\sum_{n=0}^{N-1} z_{n,m,l,l_{\mathrm{S}}} e^{\frac{j2\pi n n'}{N}} \right) \right|^{2}, \tag{13}$$

where calculating the inner sum is performed through the inverse discrete Fourier transform (IDFT) [11]. Here, each target's estimated delay is quantized using $\tau_{\mathrm{t},k,n'} = \frac{n'}{N\Delta f}$, where Δf is the subcarrier spacing.

2) DoA Estimation: This is performed through the MUSIC algorithm by utilizing the RX time-domain spatial sample vectors. Below, we also derive DoA estimation using RX frequency-domain symbols. As such, the relation between the two is shown first, needed for later derivations. This can be obtained by stacking the symbols for different subcarriers in (9) to a matrix and applying IDFT operation as

$$\begin{aligned}\mathbf{Y}_{\mathrm{r},m} &= [\mathbf{y}_{\mathrm{r},0,m},\ldots,\mathbf{y}_{\mathrm{r},N-1,m}]\mathbf{Q} \\ &= [\mathbf{A}_0(\boldsymbol{\theta})\mathbf{x}_{0,m},\ldots,\mathbf{A}_{N-1}(\boldsymbol{\theta})\mathbf{x}_{N-1,m}]\mathbf{Q}+\mathbf{V}_{\mathrm{r},m}, \quad (14)\end{aligned}$$

where the matrices $\mathbf{Y}_{\mathrm{r},m}$ and $\mathbf{V}_{\mathrm{r},m}$ are of the same size $L^{\mathrm{RF}}_{\mathrm{R,r}} \times N$, and they denote the RX time-domain samples and noise samples, respectively. The $N \times N$ IDFT matrix is represented by $\mathbf{Q} = [\mathbf{q}_0,\ldots,\mathbf{q}_{N-1}]$, where each element is given by $(\mathbf{Q})_{n,i} = (\mathbf{q}_i)_n = e^{\frac{j2\pi ni}{N}}$, with $n,i \in [0, N-1]$.

The vector of time-domain samples for the i^{th} sampling instant is given by

$$(\mathbf{Y}_{\mathrm{r},m})_i = [\mathbf{A}_0(\boldsymbol{\theta})\mathbf{x}_{0,m},\ldots,\mathbf{A}_{N-1}(\boldsymbol{\theta})\mathbf{x}_{N-1,m}]\mathbf{q}_i + (\mathbf{V}_{\mathrm{r},m})_i, \quad (15)$$

where $(\mathbf{V}_{\mathrm{r},m})_i$ is the corresponding noise vector. The covariance matrix of these samples, $\mathbf{R}_{\mathbf{Y},m,i}$, is then written as

$$\begin{aligned}\mathbf{R}_{\mathbf{Y},m,i} &= \mathbb{E}\{[\mathbf{A}_0(\boldsymbol{\theta})\mathbf{x}_{0,m},\ldots,\mathbf{A}_{N-1}(\boldsymbol{\theta})\mathbf{x}_{N-1,m}]\mathbf{q}_i\mathbf{q}_i^H \\ &\quad \cdot [\mathbf{A}_0(\boldsymbol{\theta})\mathbf{x}_{0,m},\ldots,\mathbf{A}_{N-1}(\boldsymbol{\theta})\mathbf{x}_{N-1,m}]^H\} + \sigma_{\mathrm{r}}^2\mathbf{I} \\ &= \mathbb{E}\left\{(\sum_{n=0}^{N-1} q_{i,n}\mathbf{A}_n(\boldsymbol{\theta})\mathbf{x}_{n,m})(\sum_{n=0}^{N-1} q_{i,n}^*\mathbf{x}_{n,m}^H\mathbf{A}_n^H(\boldsymbol{\theta}))\right\} + \sigma_{\mathrm{r}}^2\mathbf{I} \\ &= \sum_{n=0}^{N-1}\mathbf{A}_n(\boldsymbol{\theta})\mathbb{E}\{\mathbf{x}_{n,m}\mathbf{x}_{n,m}^H\}\mathbf{A}_n^H(\boldsymbol{\theta}) + \sigma_{\mathrm{r}}^2\mathbf{I}, \quad (16)\end{aligned}$$

where $\mathbb{E}\{\cdot\}$, σ_{r}^2 and $\mathbf{I}$ denote the expectation operation, noise variance and the identity matrix, respectively. Additionally, $q_{i,n}q_{i,n}^* = 1$, while the expectation between the frequency-domain symbols on different subcarriers becomes zero as they are assumed mutually uncorrelated.

As observed in (16), the covariance matrix of the time-domain samples is the same for all sampling instants. Moreover, assuming $\mathbb{E}\{\mathbf{x}_{n,m}\mathbf{x}_{n,m}^H\} = \sigma_x^2\mathbf{I}$, $\mathbf{R}_{\mathbf{Y},m,i}$ can be represented as $\mathbf{R}_{\mathbf{Y}}$. Utilizing (9), $\mathbf{R}_{\mathbf{Y}}$ in (16) can be written as $\mathbf{R}_{\mathbf{Y}} = \sum_{n=0}^{N-1}\mathbb{E}\{\mathbf{y}_{\mathrm{r},n,m}(\mathbf{y}_{\mathrm{r},n,m})^H\}$, and thus it can be denoted as the sum of covariance matrices of the individual subcarriers. Then, substituting from (9) results in

$$\mathbf{R}_{\mathbf{Y}} = (\mathbf{W}_{\mathrm{R,r}}^{\mathrm{RF}})^H\mathbf{A}_{\mathrm{R}}(\boldsymbol{\theta})\mathbf{R}_{\mathrm{s}}\left((\mathbf{W}_{\mathrm{R,r}}^{\mathrm{RF}})^H\mathbf{A}_{\mathrm{R}}(\boldsymbol{\theta})\right)^H + \sigma_{\mathrm{r}}^2\mathbf{I}, \quad (17)$$

where

$$\mathbf{R}_{\mathrm{s}} = \sigma_x^2\sum_{n=0}^{N-1}\mathbf{H}_{\mathrm{r},n}\mathbf{A}_{\mathrm{T}}^H(\boldsymbol{\theta})\mathbf{W}_{\mathrm{T}}^{\mathrm{RF}}\mathbf{W}_{\mathrm{T}}^{\mathrm{BB}}(\mathbf{H}_{\mathrm{r},n}\mathbf{A}_{\mathrm{T}}^H(\boldsymbol{\theta})\mathbf{W}_{\mathrm{T}}^{\mathrm{RF}}\mathbf{W}_{\mathrm{T}}^{\mathrm{BB}})^H. \quad (18)$$

The signal part of $\mathbf{R}_{\mathbf{Y}}$ in (17) will have K_{t} positive eigenvalues and $(L^{\mathrm{RF}}_{\mathrm{R,r}} - K_{\mathrm{t}})$ zero eigenvalues. Expressing each of the eigenvectors of the zero eigenvalues (null eigenvectors) as $\boldsymbol{\gamma}_l,\ l \in [1, L^{\mathrm{RF}}_{\mathrm{R,r}} - K_{\mathrm{t}}]$, it should satisfy

$$(\mathbf{W}_{\mathrm{R,r}}^{\mathrm{RF}})^H\mathbf{A}_{\mathrm{R}}(\boldsymbol{\theta})\mathbf{R}_{\mathrm{s}}\left((\mathbf{W}_{\mathrm{R,r}}^{\mathrm{RF}})^H\mathbf{A}_{\mathrm{R}}(\boldsymbol{\theta})\right)^H\boldsymbol{\gamma}_l = \mathbf{0}, \quad (19)$$

where $\mathbf{0}$ is the zero vector. This can be simplified to obtain $\left((\mathbf{W}_{\mathrm{R,r}}^{\mathrm{RF}})^H\mathbf{A}_{\mathrm{R}}(\boldsymbol{\theta})\right)^H\boldsymbol{\gamma}_l = \mathbf{0}$. Thus, the steering vectors at the RX RF chains, given by $(\mathbf{W}_{\mathrm{R,r}}^{\mathrm{RF}})^H\mathbf{a}_{\mathrm{R}}(\theta_{\mathrm{t},k})$, with $k \in [1, K_{\mathrm{t}}]$, are orthogonal to the null subspace.

From (17), it is seen that the eigenvectors of $\mathbf{R}_{\mathbf{Y}}$ are the same as those of the signal part of $\mathbf{R}_{\mathbf{Y}}$, but with increased eigenvalues due to the noise addition. Therefore to find the DoAs, eigendecomposition of $\mathbf{R}_{\mathbf{Y}}$ is performed first to find the eigenvectors corresponding to the lowest $L^{\mathrm{RF}}_{\mathrm{R,r}} - K_{\mathrm{t}}$ eigenvalues, which are then the same as $\boldsymbol{\gamma}_l$. Then, using the orthogonality condition, the MUSIC pseudo-spectrum is written as [9]

$$P(\theta) = \frac{1}{\tilde{\mathbf{a}}^H(\theta)\boldsymbol{\Gamma}\boldsymbol{\Gamma}^H\tilde{\mathbf{a}}(\theta)}, \quad (20)$$

where $\boldsymbol{\Gamma} = [\boldsymbol{\gamma}_1,\ldots,\boldsymbol{\gamma}_{L^{\mathrm{RF}}_{\mathrm{R,r}}-K_{\mathrm{t}}}]$, $\theta = [-90°, 90°]$ and $\tilde{\mathbf{a}}(\theta) = (\mathbf{W}_{\mathrm{R,r}}^{\mathrm{RF}})^H\mathbf{a}_{\mathrm{R}}(\theta)$ denotes the effective steering vector at the RX RF chains. The K_{t} highest peaks of the pseudo-spectrum will then correspond to the DoAs. To calculate $\mathbf{R}_{\mathbf{Y}}$, the sample average is used as an approximation, and is given by

$$\mathbf{R}_{\mathbf{Y}} \approx \frac{1}{MN}\sum_{m=0}^{M-1}\sum_{n=0}^{N-1}\mathbf{y}_{\mathrm{r},n,m}(\mathbf{y}_{\mathrm{r},n,m})^H. \quad (21)$$

III. JCAS MIMO Beamforming Design

In this section, we discuss how the TX BB and RF, and RX RF beamforming weights are optimized, while also canceling the SI due to full-duplex operation.

A. Proposed TX Beamforming

The TX beamforming needs to provide different effective beams for each communication user while an additional beam is used for sensing. In this work, we consider that the streams are used for both communication and sensing functionalities, however, dedicated streams could also be utilized for radar [7]. For simplicity, in this part we assume that each user has a single stream ($L_{\mathrm{S}} = 1$). Considering the presented hybrid architecture, the BB and RF weights are jointly optimized to provide multiple (viz. U) communication links while reducing the inter-user interference. In this case, we assume full control of the amplitudes and phases of these TX weights.

Based on (1)–(5), the proposed TX beamforming design maximizes the TX radar power in the radar direction θ_{r}, described as

$$\begin{aligned}P_{\mathrm{T,r}} &= \mathbb{E}\{|\mathbf{a}_{\mathrm{T}}^H(\theta_{\mathrm{r}})\mathbf{W}_{\mathrm{T}}^{\mathrm{RF}}\mathbf{W}_{\mathrm{T}}^{\mathrm{BB}}\mathbf{x}_{n,m}|^2\} \quad (22)\\ &= \sum_{u=1}^{U}|\mathbf{a}_{\mathrm{T}}^H(\theta_{\mathrm{r}})\mathbf{W}_{\mathrm{T}}^{\mathrm{RF}}\mathbf{w}_{\mathrm{T},u}^{\mathrm{BB}}|^2P_{u,n,m} = \sum_{u=1}^{U}G_{\mathrm{T,u}}(\theta_{\mathrm{r}})P_{u,n,m},\end{aligned}$$

where $\mathbf{w}_{\mathrm{T},u}^{\mathrm{BB}}$ and $P_{u,n,m} = \mathbb{E}\{|x_{u,n,m}|^2\}$ refer to the TX BB weights and the TX power of the u^{th} user's stream.

The TX BB weights of each user are optimized such that they minimize the inter-user interference, which can be perfectly canceled if $\mathbf{a}_{\mathrm{T}}^H(\theta_{\mathrm{c},u'})\mathbf{W}_{\mathrm{T}}^{\mathrm{RF}}\mathbf{w}_{\mathrm{T},u}^{\mathrm{BB}} = 0$, where $u' \neq u$. To simultaneously isolate the rest of the users U', the TX BB weights of the u^{th} user need to satisfy

$$\underbrace{[\mathbf{a}_{\mathrm{T}}^H(\theta_{\mathrm{c},1})\mathbf{W}_{\mathrm{T}}^{\mathrm{RF}},\ldots,\mathbf{a}_{\mathrm{T}}^H(\theta_{\mathrm{c},U'})\mathbf{W}_{\mathrm{T}}^{\mathrm{RF}}]}_{=\mathbf{X}_u}\mathbf{w}_{\mathrm{T},u}^{\mathrm{BB}} = \mathbf{0}. \quad (23)$$

Based on Moore–Penrose pseudoinverse's definition, a null-space projection (NSP) method can be implemented to suppress the inter-user interference [6]. Thus, the TX BB weights need to fulfill the condition

$$\mathbf{W}_{\mathrm{T}}^{\mathrm{BB}} = [\mathbf{N}_1 \hat{\mathbf{w}}_{\mathrm{T},1}^{\mathrm{BB}}, \ldots, \mathbf{N}_U \hat{\mathbf{w}}_{\mathrm{T},U}^{\mathrm{BB}}], \tag{24}$$

where $\mathbf{N}_u = (\mathbf{I} - \mathbf{X}_u^{+}\mathbf{X}_u)$ denotes the NSP matrix for the u^{th} user and $(\cdot)^{+}$ is the pseudo-inverse. The auxiliary TX BB weights $\hat{\mathbf{W}}_{\mathrm{T}}^{\mathrm{BB}} = [\hat{\mathbf{w}}_{\mathrm{T},1}^{\mathrm{BB}}, \ldots, \hat{\mathbf{w}}_{\mathrm{T},U}^{\mathrm{BB}}]$, with $\hat{\mathbf{w}}_{\mathrm{T},u}^{\mathrm{BB}}$ being any arbitrary vector of size $L_{\mathrm{T}}^{\mathrm{RF}} \times 1$, will be optimized to achieve the desired TX patterns.

The objective for optimization is to maximize the TX radar power (22) by jointly optimizing the RF and BB weights, $\mathbf{W}_{\mathrm{T}}^{\mathrm{RF}}$ and $\hat{\mathbf{W}}_{\mathrm{T}}^{\mathrm{BB}}$, and is written as

$$\max_{\hat{\mathbf{W}}_{\mathrm{T}}^{\mathrm{BB}}, \mathbf{W}_{\mathrm{T}}^{\mathrm{RF}}} \sum_{u=1}^{U} G_{\mathrm{T},u}(\theta_{\mathrm{r}}) \tag{25a}$$

$$\text{s.t.} \left\| \mathbf{W}_{\mathrm{T}}^{\mathrm{RF}} \mathbf{w}_{\mathrm{T},u}^{\mathrm{BB}} \right\| = 1, \forall u \tag{25b}$$

$$|\mathbf{a}_{\mathrm{T}}^{H}(\theta_{\mathrm{c},u}) \mathbf{W}_{\mathrm{T}}^{\mathrm{RF}} \mathbf{w}_{\mathrm{T},u}^{\mathrm{BB}}|^2 \geq \mu_u, \forall u \tag{25c}$$

$$\mathbf{W}_{\mathrm{T}}^{\mathrm{BB}} = [\mathbf{N}_1 \hat{\mathbf{w}}_{\mathrm{T},1}^{\mathrm{BB}}, \ldots, \mathbf{N}_U \hat{\mathbf{w}}_{\mathrm{T},U}^{\mathrm{BB}}], \tag{25d}$$

where the effective TX weights of each user are normalized with (25b) to constrain the TX power. The required TX gain for each user μ_u is imposed by the communication system with (25c). In addition, the NSP constraint (25d) reduces the inter-user interference according to (24).

To obtain numerical results, in the next section, we solve the above constrained beamforming optimization using the optimization toolbox of MATLAB.

B. RX Beamforming

In the RX side, a single beam is required to sense the radar direction, while SI is to be effectively suppressed as illustrated in Fig. 1. In this case, we optimize the RX RF weights at the different RF chains separately. The effective SI channel between each TX stream and RX RF chain is given by

$$\hat{\mathbf{H}}_{\mathrm{SI},n} = (\mathbf{W}_{\mathrm{R,r}}^{\mathrm{RF}})^{H} \mathbf{H}_{\mathrm{SI},n} \mathbf{W}_{\mathrm{T}}^{\mathrm{RF}} \mathbf{W}_{\mathrm{T}}^{\mathrm{BB}}, \tag{26}$$

where $\{\hat{\mathbf{H}}_{\mathrm{SI},n}\}_{l_{\mathrm{R}}^{\mathrm{RF}},u}$ with $u \in [1, U]$ and $l_{\mathrm{R,r}}^{\mathrm{RF}} \in \left[1, L_{\mathrm{R}}^{\mathrm{RF}}\right]$. Similar to (24), an NSP method is implemented to cancel the frequency-dependent SI in (26). As mm-wave JCAS systems are most likely having large bandwidths in order to provide high data rates and highly accurate radar measurements, we consider an NSP method which implements $\mathcal{N}_{\text{freq}}$ frequency nulls in the operating band. Therefore, the RX RF weights $\mathbf{w}_{\mathrm{R,r},l_{\mathrm{R}}^{\mathrm{RF}}}^{\mathrm{RF}}$ for the $l_{\mathrm{R}}^{\mathrm{RF}}$th subarray need to satisfy

$$(\mathbf{w}_{\mathrm{R,r},l_{\mathrm{R}}^{\mathrm{RF}}}^{\mathrm{RF}})^{H} \underbrace{\left[\mathbf{H}_{\mathrm{SI},1} \mathbf{W}_{\mathrm{T}}^{\mathrm{RF}} \mathbf{W}_{\mathrm{T}}^{\mathrm{BB}}, \ldots, \mathbf{H}_{\mathrm{SI},\mathcal{N}_{\text{freq}}} \mathbf{W}_{\mathrm{T}}^{\mathrm{RF}} \mathbf{W}_{\mathrm{T}}^{\mathrm{BB}}\right]}_{=\mathbf{X}_{l_{\mathrm{R}}^{\mathrm{RF}}}} = \mathbf{0}^{T}, \tag{27}$$

where $\mathbf{W}_{\mathrm{R,r}}^{\mathrm{RF}} = [\mathbf{w}_{\mathrm{R,r},1}^{\mathrm{RF}}, \ldots, \mathbf{w}_{\mathrm{R,r},L_{\mathrm{R}}^{\mathrm{RF}}}^{\mathrm{RF}}]$. Similar to [6], the RF RX weights of each subarray are optimized to maximize the RX gain at the radar direction $G_{\mathrm{R}}(\theta_{\mathrm{r}}) = |(\mathbf{w}_{\mathrm{R,r},l_{\mathrm{R}}^{\mathrm{RF}}}^{\mathrm{RF}})^{H} \mathbf{a}_{\mathrm{R}}(\theta_{\mathrm{r}})|^2$, while effectively suppressing the SI at the desired frequencies. Then, the final weights are described as [6]

$$\mathbf{w}_{\mathrm{R,r},l_{\mathrm{R}}^{\mathrm{RF}}}^{\mathrm{RF}} = \frac{(\mathbf{I} - \mathbf{X}_{l_{\mathrm{R}}^{\mathrm{RF}}} \mathbf{X}_{l_{\mathrm{R}}^{\mathrm{RF}}}^{+}) \mathbf{a}_{\mathrm{R}}(\theta_{\mathrm{r}})}{\left\| (\mathbf{I} - \mathbf{X}_{l_{\mathrm{R}}^{\mathrm{RF}}} \mathbf{X}_{l_{\mathrm{R}}^{\mathrm{RF}}}^{+}) \mathbf{a}_{\mathrm{R}}(\theta_{\mathrm{r}}) \right\|}. \tag{28}$$

IV. Numerical Results

Numerical evaluations are next carried out to demonstrate the performance of the proposed MIMO JCAS system, by considering a hybrid architecture. In the following results, realistic linear patch antenna arrays simulated with CST Studio Suite are used. In addition, the simulated arrays incorporate the mutual coupling effects that model the SI in a band with center frequency of $f_{\mathrm{c}} = 28$ GHz and bandwidth of 500 MHz.

Figure 2 shows illustrative examples of the proposed MU-MIMO JCAS beamforming with two communication links at -30° and 40°, while an additional beam at 10° is used for sensing. As it can be observed in Fig. 2(a), streams from different UEs experience different effective TX patterns depending on their TX BB weights. Moreover, all the streams are transmitted towards the radar direction. The effective pattern of each user minimizes the inter-user interference by imposing nulls in the other user's directions. On the RX side, a separate design of the RF weights of each subarray is implemented to maximize the radar gain as shown in Fig. 2(b). In addition, these weights are optimized to efficiently suppress the wideband SI signal by implementing multiple frequency nulls as illustrated in Fig. 2(c).

Next, RX MIMO processing is applied for estimating the range and angle profiles using similar simulation parameters as in Fig. 2 considering $L_{\mathrm{R,r}}^{\mathrm{RF}} = 8$ (i.e., eight RX RF chains). Separate point targets are placed at each communication direction (-30° and 40°), while two more are placed at the radar direction, with a 2° angular separation (10° and 12°). Additionally, the communication users are at different ranges, but the radar targets have almost the same range. A standard-compliant 5G OFDM waveform is then used at the MIMO TX with the following parameters: one OFDM symbol, $N = 3168$ and $\Delta f = 120$ kHz. Then, the RX spatial signal is used for range and DoA estimation as described in Section II-B.

Figure 3(a) depicts a range profile corresponding to the targets. Although there are four separate targets, the range profile depicts only three, where the two radar targets are shown as one. This is because the bandwidth of the waveform is not high enough to differentiate between the two radar targets that are very closely situated in range. To observe if the targets can be differentiated in angular domain, the MUSIC pseudo-spectrum is calculated according to (20) for finding the angle profile of the targets. Figure 3(b) depicts that four separate directions can be estimated in the angle profile. Due to the super-resolution DoA estimation, it can additionally be observed that there exist two radar targets. It should be stated here that the DoAs are still not associated with the ranges directly though since the range and angle profiles are estimated separately.

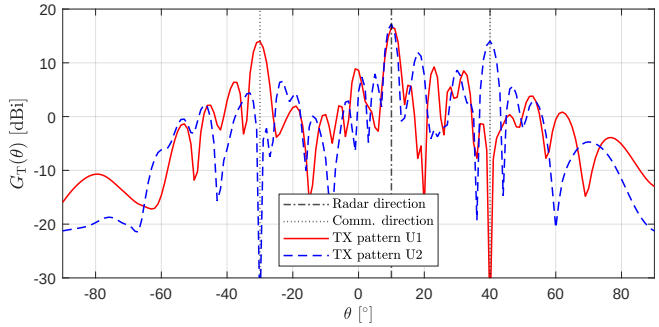

(a) Effective TX pattern for each stream

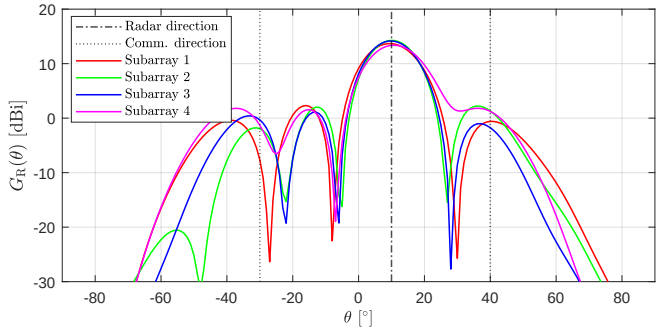

(b) Subarrays' RX patterns

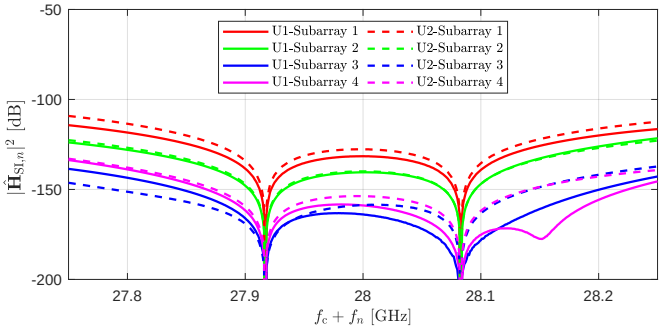

(c) SI frequency response

Fig. 2. Illustration of JCAS MIMO performance with a radar beam at $\theta_{\mathrm{r}} = 10°$ and two communication users (U1 and U2) located at $\theta_{\mathrm{c},1} = -30°$ and $\theta_{\mathrm{c},2} = 40°$, respectively. The rest of simulation parameters are $U = 2$, $L_{\mathrm{S}} = 1$, $L_{\mathrm{T}} = 32$, $L_{\mathrm{R,r}} = 32$, $L_{\mathrm{T}}^{\mathrm{RF}} = 8$, $L_{\mathrm{R,r}}^{\mathrm{RF}} = 4$, and $\mathcal{N}_{\mathrm{freq}} = 2$.

V. Conclusion

In this article, we addressed the beamforming optimization and other related signal processing aspects in a hybrid MIMO JCAS system context. The TX BB and RF beamforming weights were optimized to provide multiple simultaneous beams for communication and sensing while suppressing the inter-user interference between different users. The RX RF beamforming was optimized to receive reflections from the sensing direction while minimizing the SI due to full-duplex operation. Additionally, the RX spatial signal was used to estimate the range and angle profiles corresponding to the targets. The results indicate that TX and RX beampatterns can be optimized for improved performance of the JCAS system. Moreover, the DoA estimation allows to separate multiple targets with the same range within the sensing beam.

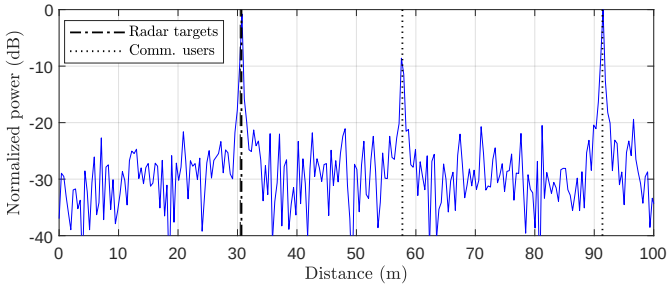

(a) Range profile

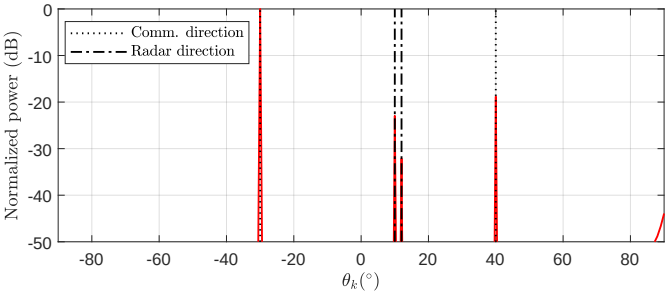

(b) Angle profile

Fig. 3. The estimated range and angle profiles for the simulated scenario with angles $\theta_{\mathrm{c},1} = -30°, \theta_{\mathrm{c},2} = 40°, \theta_{\mathrm{t},1} = 10°, \theta_{\mathrm{t},2} = 12°$, and ranges $\mathrm{d}_{\mathrm{c},1} = 57.74\mathrm{m}, \mathrm{d}_{\mathrm{c},2} = 91.38\mathrm{m}, \mathrm{d}_{\mathrm{t},1} = 30.46\mathrm{m}, \mathrm{d}_{\mathrm{t},2} = 30.67\mathrm{m}$.

References

[1] F. Liu, C. Masouros, A. P. Petropulu, H. Griffiths, and L. Hanzo, "Joint radar and communication design: Applications, state-of-the-art, and the road ahead," *IEEE Trans. Commun.*, vol. 68, no. 6, pp. 3834–3862, Feb. 2020.

[2] S. A. Busari, K. M. S. Huq, S. Mumtaz, L. Dai, and J. Rodriguez, "Millimeter-wave massive MIMO communication for future wireless systems: A survey," *IEEE Commun. Surveys Tuts.*, vol. 20, no. 2, pp. 836–869, Dec. 2017.

[3] F. Liu, C. Masouros, A. Li, H. Sun, and L. Hanzo, "MU-MIMO communications with MIMO radar: From co-existence to joint transmission," *IEEE Trans. Wireless Commun.*, vol. 17, no. 4, pp. 2755–2770, Apr. 2018.

[4] S. Biswas, K. Singh, O. Taghizadeh, and T. Ratnarajah, "Design and analysis of FD MIMO cellular systems in coexistence with MIMO radar," *IEEE Trans. Wireless Commun.*, vol. 19, no. 7, pp. 4727–4743, Jul. 2020.

[5] Y. L. Sit, C. Sturm, J. Baier, and T. Zwick, "Direction of arrival estimation using the MUSIC algorithm for a MIMO OFDM radar," in *Proc. IEEE Radar Conf.*, May 2012, pp. 226–229.

[6] C. Baquero Barneto *et al.*, "Beamforming and waveform optimization for OFDM-based joint communications and sensing at mm-waves," in *Proc. Asilomar Conf. on Signals, Syst., Comput.*, Nov. 2020.

[7] X. Liu, T. Huang, N. Shlezinger, Y. Liu, J. Zhou, and Y. C. Eldar, "Joint transmit beamforming for multiuser MIMO communications and MIMO radar," *IEEE Trans. Signal Process.*, vol. 68, pp. 3929–3944, Jun. 2020.

[8] C. Baquero Barneto, S. D. Liyanaarachchi, M. Heino, T. Riihonen, and M. Valkama, "Full-duplex radio/radar technology: The enabler for advanced joint communication and sensing," *IEEE Wireless Commun.*, Feb. 2021.

[9] R. Schmidt, "Multiple emitter location and signal parameter estimation," *IEEE Trans. Antennas Propag*, vol. 34, no. 3, pp. 276–280, Mar. 1986.

[10] R. W. Heath, N. González-Prelcic, S. Rangan, W. Roh, and A. M. Sayeed, "An overview of signal processing techniques for millimeter wave MIMO systems," *IEEE J. Sel. Topics Signal Process.*, vol. 10, no. 3, pp. 436–453, Apr. 2016.

[11] S. D. Liyanaarachchi, C. B. Barneto, T. Riihonen, and M. Valkama, "Joint OFDM waveform design for communications and sensing convergence," in *Proc. IEEE Int. Conf. on Commun.*, Jun. 2020.